Optics and Lasers in Engineering 67 (2015) 22–30

Contents lists available at ScienceDirect

Optics and Lasers in Engineering

journal homepage: www.elsevier.com/locate/optlaseng

Application of laser in seam welding of dissimilar steel to aluminium joints for thick structural components

S. Meco [a,*], G. Pardal [a], S. Ganguly [a], S. Williams [a], N. McPherson [b]

[a] Welding Engineering and Laser Processing Centre, Cranfield University, University Way (Building 46), Bedford, MK43 0AL, United Kingdom
[b] BAE Systems Maritime – Naval Ships, 1048 Govan Road, Glasgow, G14 5XP, United Kingdom

ARTICLE INFO

Article history:
Received 25 April 2014
Received in revised form
23 August 2014
Accepted 19 October 2014

Keywords:
Laser welding-brazing
Conduction
Intermetallic compound
Steel
Aluminium alloy

ABSTRACT

Laser welding-brazing technique, using a continuous wave (CW) fibre laser with 8000 W of maximum power, was applied in conduction mode to join 2 mm thick steel (XF350) to 6 mm thick aluminium (AA5083-H22), in a lap joint configuration with steel on the top. The steel surface was irradiated by the laser and the heat was conducted through the steel plate to the steel-aluminium interface, where the aluminium melts and wets the steel surface. The welded samples were defect free and the weld micrographs revealed presence of a brittle intermetallic compounds (IMC) layer resulting from reaction of Fe and Al atoms. Energy Dispersive Spectroscopy (EDS) analysis indicated the stoichiometry of the IMC as Fe_2Al_5 and $FeAl_3$, the former with maximum microhardness measured of 1145 HV 0.025/10. The IMC layer thickness varied between 4 to 21 μm depending upon the laser processing parameters. The IMC layer showed an exponential growth pattern with the applied specific point energy (E_{sp}) at a constant power density (*PD*). Higher *PD* values accelerate the IMC layer growth. The mechanical shear strength showed a narrow band of variation in all the samples (with the maximum value registered at 31.3 kN), with a marginal increase in the applied E_{sp}. This could be explained by the fact that increasing the E_{sp} results into an increase in the wetting and thereby the bonded area in the steel-aluminium interface.

1. Introduction

In recent past the surface transportation industry has been challenged to reduce fuel consumption and to comply with the governmental policies to lower the carbon emissions. To achieve these objectives, fuel efficient engines and mass efficient structural materials, aiming to reduce the total weight of the vehicle, are required. Therefore, light alloys are increasingly in use along with the traditional structural materials in vehicle designs. Aluminum (Al) is one of the materials of choice as it is cost effective, has high specific modulus and is corrosion resistant. The latest design solutions are aimed at using a higher proportion of Al as a structural material. Therefore, a cost effective and energy efficient joining solution with steel and Al would be vital to realize the potential of such innovative design solutions. The main issues associated with the joining of steel to Al are their different physical properties (e.g. melting temperatures, thermal expansion and conductivity), the nearly zero solid solubility of Al in iron (Fe) and zero solid solubility of Fe in Al and the resulting formation of intermetallic compounds (IMC). The diffusion of Fe and Al atoms at the Fe-Al interface forms different types of IMCs that are harmful for the structure due to their brittle behaviour. The most frequently reported IMCs are $FeAl_3$ and Fe_2Al_5.

Many studies have been carried out with the goal of understanding and minimizing the Fe-Al reaction. Some researchers were focused on the study of Fe-Al reaction between molten Al and solid steel, controlling the time-temperature and evaluating the IMC layer composition and growth [1–3], whilst others assessed the influence of other alloying elements on the IMC layer thickness growth [4,5]. The research developed by Shih et al. is an example of the latter point, where a steel bar was dipped in different molten Al alloys (pure, Si, Mg and Si-Mg based) during different time intervals, to evaluate the influence of these elements on the Fe-Al reaction [5]. The Al alloy containing Si and Mg showed the thinnest IMC layer.

The physical state of the alloys (solid or liquid) at the joint interface during the joining process is one of the determining factors for the formation of IMC because it directly controls the activity and mobility of the atoms of the participating alloys.

In solid state joining processes, such as friction stir welding [6] or linear friction welding [7], the formation of the Fe-Al IMC is usually minimized because there is basically only plastic deformation of the Al and the temperature generated during the joining process is very low (usually lower than the melting temperature of

* Corresponding author. Tel.: +44 0 1234750111.
E-mail addresses: s.a.martinsmeco@cranfield.ac.uk (S. Meco), g.n.rodriguespardal@cranfield.ac.uk (G. Pardal), s.ganguly@cranfield.ac.uk (S. Ganguly), s.williams@cranfield.ac.uk (S. Williams), norrie.mcpherson@baesystems.com (N. McPherson).

http://dx.doi.org/10.1016/j.optlaseng.2014.10.006
0143-8166/

the substrate). Explosion welding has another advantage, as the process happens so quickly there is almost no time for the reaction between Fe and Al and so the IMC layer is also very thin as demonstrated in [8–10].

Laser welding-brazing technique produces a joint between solid steel and molten Al [11–14] and is usually applied with filler wire. The interaction between both metals using this technique is minimal and consequently, sound dissimilar joints are produced with mechanical strength either identical or close to the weaker of the two metals (steel or Al plate, depending on the cross-sectional area of the specimen). An alternative technique was assessed in which a rolling system was combined to the laser [15–17]. The principle of this technique is to heat the substrate with the laser and immediately apply pressure on the soft metal with a roller to improve the contact in hot stage and thus the bonding. This way sound joints could be produced with IMC layer thickness less than 10 μm (many researchers have considered 10 μm as a reference maximum value of IMC layer thickness for an acceptable steel to Al joint [18]). Resistance spot welding applied to the steel to Al joining was also investigated [19–22]. Even though this process is a solid state pressure welding process, the researchers couldn't prevent formation of the IMCs and the samples failed from the interface when tested under tensile loading.

On the other hand, when both metals are in liquid state during the joining process, as is the case of the high power laser welding in keyhole mode [23–25], thick Fe-Al IMC layers are formed due to uncontrolled reaction and the joints are fragile.

It is well known from previous studies that the Fe-Al reaction depends on the welding temperature and time. IMC formation and growth is favoured when the welding thermal cycle is prolonged. This is expected because formation of IMC is a diffusion controlled process and prolonged time and higher temperature will allow more diffusion. Borrisutthekul et al. observed that under such conditions the IMC layer becomes thicker and as a result the joint mechanical strength would be lower [26].

So far in the area of joining this specific dissimilar combination, most of the research focus is towards the automotive industry and therefore, only thin (~1 mm) sheets of steel and Al have been investigated. For maritime application, where thick (>3 mm) plates are used, only few papers were found, for instance the work produced by Thomy et al. using the laser-MIG hybrid process to join 3 mm plates of steel and Al in a butt joint configuration [27]. At present, in many industrial applications an explosion bonded hybrid transition bar, half Al and other half Fe, is used for successful joining of steel and Al (Fig. 1). However, the resulting joining process is not cost effective as it increases the cost of production through the cost of the bar and complicated logistics of operation. In addition, four fillet welds were necessary when a transition bar is used, instead of two, if Fe and Al were joined directly. The cost effectiveness and mass efficiency are thus reduced in such structures.

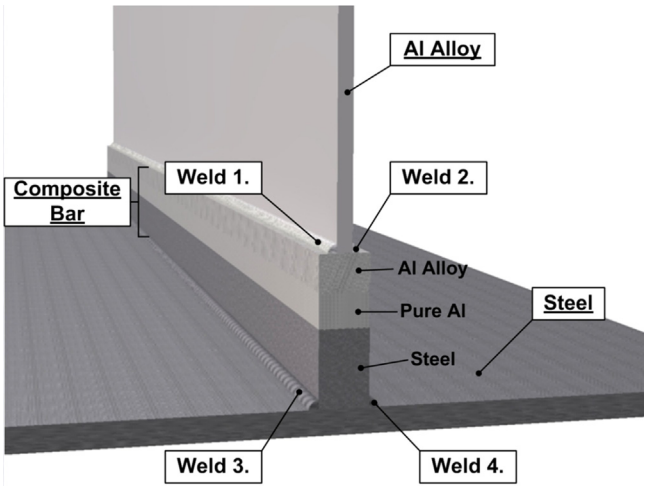

Fig. 1. Schematic representation of the dissimilar metal joint of steel to aluminium with the transition bar

The overall aim of the present research programme is to develop a process in which thick plates of steel can be joined directly to Al without application of a filler material. Application of laser to join steel to aluminium in overlap configuration by welding-brazing process was investigated where the laser applied on the steel surface is conducted through and melts the aluminium to wet the steel surface. This minimizes random mixing of the two alloys as steel remains in solid state. However, in order to achieve viable joint it is necessary to understand the underpinning interaction between the laser source and the alloys and correlate the microstructural constituents of the interface with the interaction parameters and finally to the mechanical strength of the joint. This will enable development of a cost effective, design and energy efficient joining solution between Fe and Al with appropriate mechanical strength and metallurgical characteristics suitable for the intended application. In order to achieve this, an experimental matrix based on fundamental laser material interaction parameters was defined and the growth of Fe-Al IMC is correlated with the transient thermal (time-temperature) cycle resulting from the laser-material interaction.

2. System Parameters versus fundamental material interaction Parameters

In research and industrial application of laser welding, the vast majority of results is presented in terms of the laser system parameters, such as laser power (P), laser beam diameter (D_{beam}) and travel speed (TS). However, these parameters alone are not sufficient to describe the interaction of the laser beam with the material. Welding experiments using the fundamental material interaction parameters ($FMIP$), which include power density (PD), interaction time (t_i) and specific point energy (E_{sp}), have proven to be able to fully characterize the laser welding process [28].

As mentioned before, when a laser beam interacts with a material the total energy input cannot be controlled by individual control of either of these three parameters. Within the defined fundamental laser material interaction parameters, power density is defined as the ratio of the power to the applied area of the spot as shown in Eq. (1). This parameter is one of the chief determinant of welding mode (conduction and keyhole) [29]. Interaction time is defined by the ratio of laser travel speed to the spot size and signifies the irradiation time of an infinitesimal element within the laser spot. Calculation of interaction time (t_i) is shown in Eq. (2). The total laser energy delivered within a spot designated here as specific point energy is shown in Eq. (3) which is the product of power density, interaction time and the total area of the spot [30].

$$\text{Power density } [W.\text{m}^{-2}] = \frac{\text{Laser Power}}{\text{Area}_{\text{beam}}} \quad (1)$$

$$\text{Interaction time } [\text{s}] = \frac{\text{Diameter}_{\text{beam}}}{\text{Travel speed}} \quad (2)$$

$$\text{Specific point energy } [\text{kJ}] = \text{Power density} \times \text{Interaction time} \times \text{Area}_{\text{beam}} \quad (3)$$

Researchers investigated on FMIP emphasized that parameters developed in this process are transferrable between different laser systems [31] and shown direct correlation between FMIP, thermal profile and weld metal geometric profile.

Table 1
Chemical composition of base materials

Material	Elements (wt. %)												
	Al	Fe	C	Si	Mn	P+S	Ni	Ti	Cu	Mg	Zn	Cr	Other
XF350	0.047	Bal.	0.059	0.021	0.610	0.025	0.020	0.001	0.03	–	–	0.030	0.255
5083-H22	Bal.	0.400	–	0.400	0.500	–	–	0.150	0.100	2.600–3.600	0.200	0.300	–

Table 2
Mechanical properties of base materials

Material	Yield strength [MPa]	Ultimate tensile strength [MPa]
XF350	368	474
5083-H22	250	337

3. Material and methods

3.1. Materials

The materials used in the experiments were 2 mm thick XF350 high strength low alloy steel and 6 mm thick 5083H22 aluminium. The chemical composition and mechanical properties of the materials are depicted in Table 1 and Table 2, respectively.

3.2. Experimental principle

As discussed before, laser welding-brazing principle has been applied in the present work. This technique is possible to apply in a lap joint configuration with steel on aluminium, since both materials have dissimilar thermal properties (thermal conductivity and melting temperature). In other words, when steel is on top of aluminium, the positive gradient on thermal conductivity allows the heat to flow downwards in the thickness direction. As the melting temperature of aluminium is significantly lower than that of steel it is possible to melt the aluminium alone and wet the interface while maintaining the steel in the solid state. The experimental hypothesis is schematically explained in Fig. 2.

The geometry of the fusion zone visible in Fig. 2 is characteristic of a weld produced with a laser in conduction mode. By definition, the aspect ratio (penetration depth by weld width) must be smaller than 0.5 [32] and the power density must be lower than 10^6 W.cm^{-2} [33] for a weld to be considered in conduction mode. In this work, both conditions were verified and all joints were produced in conduction mode. Using such mode the process is more stable and allows appropriate temperature gradients to establish between the dissimilar alloys to ensure melting of the aluminium only. As can be understood, keyhole mode (the other variant of the laser process) is not suitable for such joining process as keyhole mode is less flexible as the temperature reaches more than vapourisation temperature and therefore, it will be impossible to control melting of the steel and thereby mixing of the two alloys. Other consequence of the keyhole mode is the number of defects formed during the welding process, such as porosities due to the gas entrapment during the solidification of the weld pool and undercuts due to metal projection [31,34].

3.3. Experimental setup

Samples of steel and aluminium with 138 mm width and 200 mm long were linished just before welding, to remove the oxides on the metal surface, and then degreased with acetone. The steel plate was positioned on top of the aluminium plate in a lap joint configuration, with an overlap of 46 mm. A toggle clamping device was developed to ensure no macroscopic gap between the two plates and thus, to ensure the best possible heat conduction through the steel plate to the aluminium, along the weld seam. The toggle clamping device also ensured identical pressure in all the experiments and also contributed to a more efficient setup in terms of time (Fig. 3).

The laser head was fixed to a Fanuc robot, which was kept stationery during the joining process.The weld seams were produced by the linear movement of the gantry table, on which the samples were mounted. The weld area was shielded with inert argon gas with 20 l.min^{-1} flow rate. No filler material or flux was used in the experiments.

The seam welds were done using a fibre laser, with 8000 W of maximum power, in conduction mode by using a defocused laser beam. A focusing lens of 500 mm was used with a distance between the laser head and the workpiece of 774 mm. The values of the system and fundamental material interaction parameters used in the experiments are shown in Table 3. The latter parameters are calculated using the system parameters as shown in Section 1 of this article (Eqs. (1)–(3)).

The values of the parameters indicated in Table 3 result from a number of experiments produced prior to identify the laser system parameters to produce good welds. A combination of a laser beam with 13 mm of diameter and laser power of 4 kW and 5 kW was considered for conduction welding mode. The minimum travel speed for each laser power corresponds just before having the entire thickness of the steel plate melted, whereas the maximum travel speed corresponds to the limit from which no bonding is produced.

3.4. Microstructure and mechanical Tests

The experimental error of the welding process was calculated based on two samples welded under the same condition. Then, the welded specimens were machined to take three samples from each weld – one for mechanical test and the other two for microanalysis.

The microstructure of the welded samples was observed in an optical microscope and also in a scanning electron microscope. The SEM with an integrated energy-dispersive X-ray spectroscopy was also used for a semi-quantitative compositional analysis of the IMC.

To determine the IMC layer thickness, a series of micrographs was taken at 40x magnification of the objective lens. Then, the average of the IMC layer thickness was taken from each picture using the Axion vision software. The maximum thickness of the IMC layer corresponded to the maximum average calculated.

Microhardness tests were done with the Zwick/Roell type ZHV microhardness equipment, using 25 g of load with loading duration of 10 s.

To quantify the joint strength of the lap welds, tensile shear strength tests were performed using the electro-mechanical equipment (Instron 5500 R) with 100 kN load cell. The tests were carried out at room temperature with 1 mm.s^{-1} cross head speed. The cross weld lap shear test specimens were straight-sided and 60 mm wide and 230 mm long.

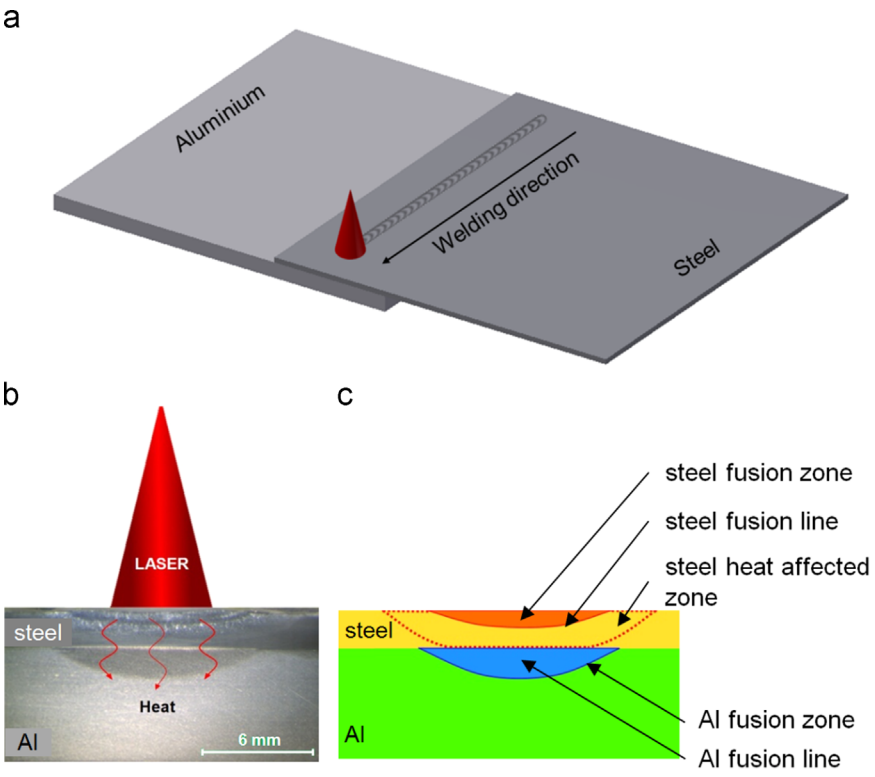

Fig. 2. Schematic representation of the laser welding-brazing process: (a) general view, (b) macroscopic cross section view and (c) identification of the different metallurgical zones

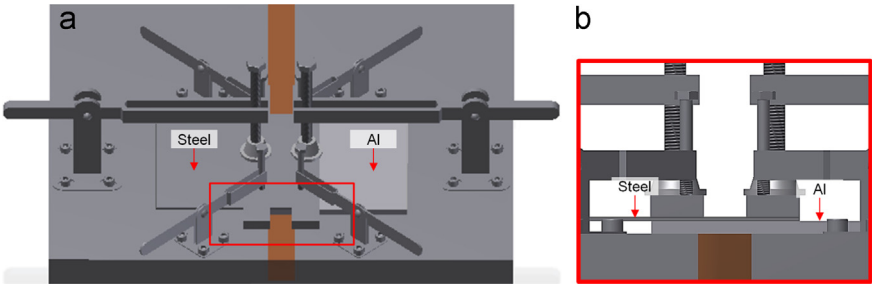

Fig. 3. Clamping system used in laser welding-brazing with the lap joint configuration: (a) General view, (b) detailed view

Table 3
System and fundamental material interaction parameters used in the laser welding-brazing experiments

System parameters			Fundamental material interaction parameters		
Beam diameter, D_{beam} [mm]	Power, P [kW]	Travel speed, TS [m.min^{-1}]	Power density, PD [kW.m^{-2}]	Interaction time, t_i [s]	Specific point energy, E_{sp} [kJ]
13	4	0.20		3.90	15.60
		0.25	3.01E+4	3.12	12.48
		0.30		2.60	10.40
	5	0.30		2.60	13.00
		0.35	3.77E+4	2.23	11.14
		0.40		1.95	9.75

4. Results and discussion

4.1. Macro and microstructure

Fig. 4(a) shows a cross section of a weld. It can be seen that the steel was partially melted near the top where it was irradiated by the laser, however, near the Fe-Al interface the steel remained in the solid state. This happened in all the experiments, even in the samples produced with 9.75 kJ the lowest specific point energy (E_{sp}) (see Table 3), since to ensure the temperature on the Fe-Al interface is higher than aluminum melting point, the temperature gradient across the steel plate thickness needs to be sufficiently high, melting occurs at the steel top surface.

Micrographs in Fig. 4(b) show the presence of the IMC layer formed by the Fe-Al reaction. The IMC layer thickness is not uniform along the cross section. Micrograph I and III in Fig. 4(b) correspond to the edges of the weld and show relatively thinner IMC layer as compared to the centre (micrograph II in Fig. 4(b)) where the IMC layer is thicker. This can be attributed to the differential thermal cycle near the edge and the centre of the weld. Near the centre, the temperature is higher and the cooling rate is lower whilst in the edges the temperature is lower and the cooling rate is higher. Three factors may be responsible for this: (1) the surrounding material that extracts the heat from the weld zone and (2) the intensity profile of the laser beam that induces the highest temperature near the centre of the weld and (3) the fact that the interaction time is highest near the centre of the weld. According to the literature, the IMC formation is diffusion controlled and thereby dependent on the time and temperature characteristics of the process.

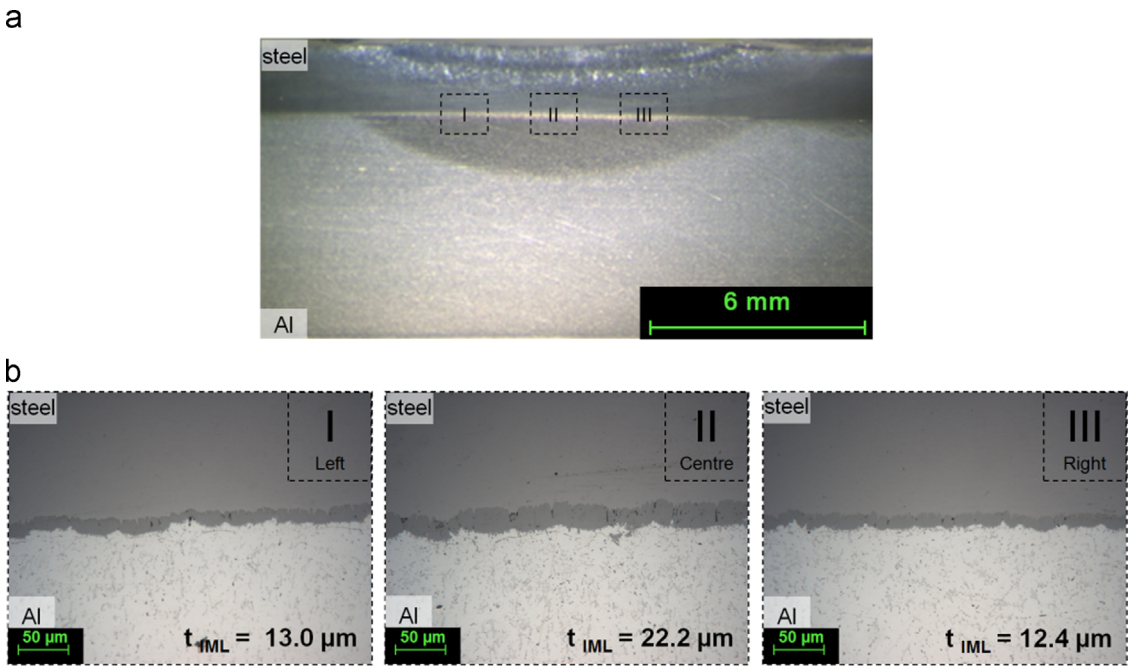

Fig. 4. Evolution of IMC layer thickness along the cross section (P=4.0 kW; TS=0.20 m.min-1; Dbeam=13 mm; PD=3.01E+4 k W.m-2; ti=3.9 s; Esp=15.6 kJ): (a) Macrosection; (b) Microsections

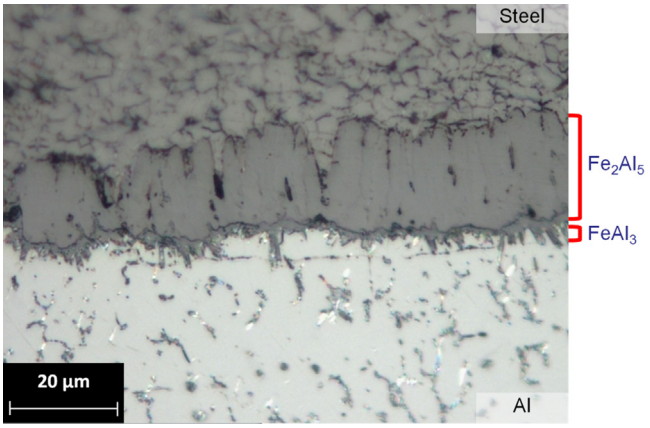

Fig. 5. Optical micrograph showing two distinct layers in the IMC layer

The IMC layer is composed of two distinct layers (Fig. 5). The IMC present in these layers are $FeAl_3$ on the aluminium side and Fe_2Al_5 on the steel side. As referred by [20], [35] and [36], the $FeAl_3$ layer is usually thin and present as a needle shape morphology whilst the Fe_2Al_5 layer is usually thicker than the latter and tongue shape but strongly dependent on time-temperature. At the edges, where the temperature is lower as well as the interaction time, there is only the $FeAl_3$ layer. According to Qiu et al. [22], $FeAl_3$ IMC has lower free energy of formation than other IMC and, thus its formation is easier in terms of thermodynamic principles. However, the kinetic aspect of the Fe_2Al_5 formation is more favourable. This explains the nearly constant thickness of $FeAl_3$ in contrast to the irregular thickness of Fe_2Al_5 layer across the weld.

The composition of the two IMC layers was identified by EDS spectrum analysis (Fig. 6). The EDS results confirmed the IMC previously identified based on the morphology: the needle shape $FeAl_3$ with 62% Al and thicker tongue shaped layer of Fe_2Al_5 with 56% Al.

The same morphology is seen in the SEM micrographs (Fig. 7(a)) but the two layers are not clearly distinguishable. The highlighted dots in the EDS mapping of Fig. 7(b) and Fig. 7(c) correspond to the Fe and Al elements, respectively. The lower concentration of dots in

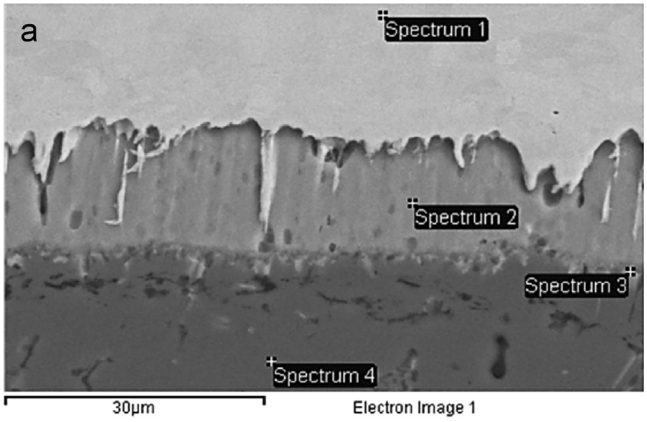

b

Weight %	Fe	Al	Mg	Phases
Spectrum 1	100	-	-	Fe
Spectrum 2	44.42	55.58	-	Fe_2Al_5
Spectrum 3	38.12	61.88	-	$FeAl_3$
Spectrum 4	-	95.28	4.72	Al

Fig. 6. EDS spectrum analysis

the centre of both pictures forming a horizontal band is explained by the presence of the Fe-Al IMC (Fe and Al elements were detected simultaneously in that region during the EDS analysis).

Microhardness testing was carried out along a vertical line in the cross sectional plane extending to both the parent metals as shown in Fig. 8. The irregular behaviour on the hardness curve on the steel side is due to the partial melting of the material near the top that resulted into different metallurgical phase formations as compared to the part which remained solid throughout the process. On the Al side the hardness value showed very consistent and uniform result around 70 HV 0.025/10. As expected, the maximum value of hardness was observed on the IMC layer with 1145 HV 0.025/10. This value is similar to the one reported by Olsen [35], 1100 HV.

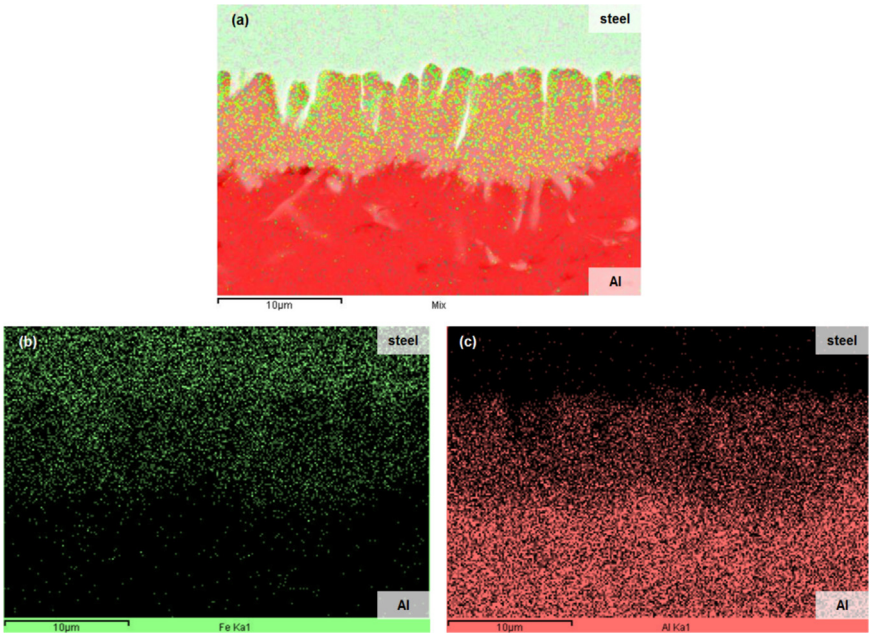

Fig. 7. EDS mapping pictures: (a) Mix of Fe and Al elements, (b) Fe elements, (c) Al elements

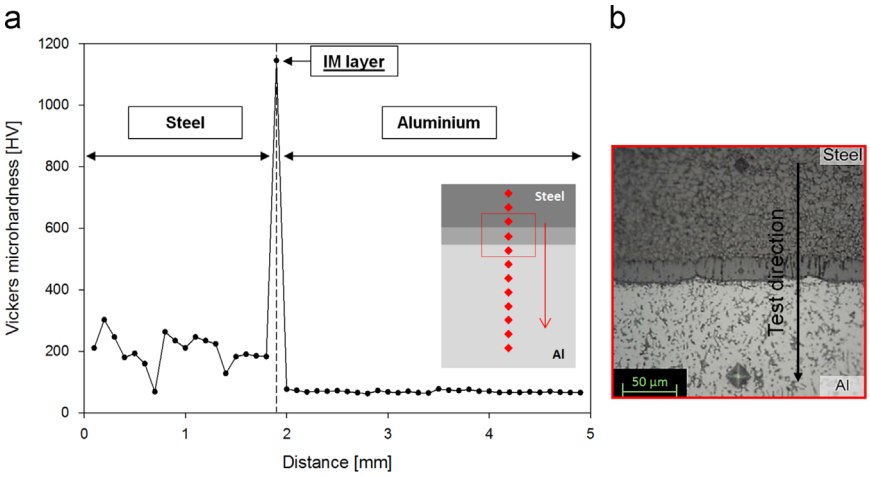

Fig. 8. (a) Microhardness distribution along the thickness of the sample and (b) microscopic view of the indentations near the Fe-Al interface

Fig. 8(b) shows a micrograph where the microindentation on the IMC Fe_2Al_5 is visible. As the $FeAl_3$ IMC layer is very thin, about 2 μm, it was not possible to measure the hardness with the microindenter.

4.2. Laser welding process

As mentioned in section 3.2, the experiments were carried out in conduction mode with the laser beam incident on the steel plate through which heat was conducted, melting the aluminum and bonding the two metals. Using this methodology, the temperature in the Fe-Al interface is lower than the melting point of the steel and as steel was maintained in solid state, the diffusion of Fe and Al elements is minimized and thus, the Fe-Al reaction was reduced.

The visual inspection on the welds produced with laser process in conduction mode revealed no defects which was in agreement with [31,34] – the weld seam was uniform with neither porosities nor cracks.

Laser welding-brazing applied in joining of thick plates of steel to aluminium, compared to other joining processes, such as hybrid laser-arc welding, has better process control in terms of energy transferred to the work piece and has lower complexity because it has less parameters to control. Another example is the explosion welding process in which the resultant welds have good mechanical properties due to the low levels of IMC layer thickness but the process is much less versatile in terms of material and geometries to weld than laser welding [9].

Fig. 9 shows the micrographs of the cross section of the samples welded under different welding conditions: two different power density (*PD*) values and three different specific point energy (E_{sp}) values.

Fig. 10 shows the evolution of the IMC layer thickness with specific point energy which was varied by changing either the power density or the interaction time to understand effect of these parameters independently. The error bars represented in the graph correspond to the variance of IMC layer thickness measured in two samples taken from two joints produced under identical welding conditions. The experimental results are considered to be acceptable since the variation of IMC layer thickness produced under different energy levels falls outside the error bars.

The point worth mentioning is the similar pattern of the two curves with the different *PD* values (Fig. 10). The growth of IMC layer shows an exponential trend with the E_{sp}. It can be clearly seen that as the E_{sp} increases, IMC layer growth increases. This is expected as thermal cycle prolongs with increase in energy input.

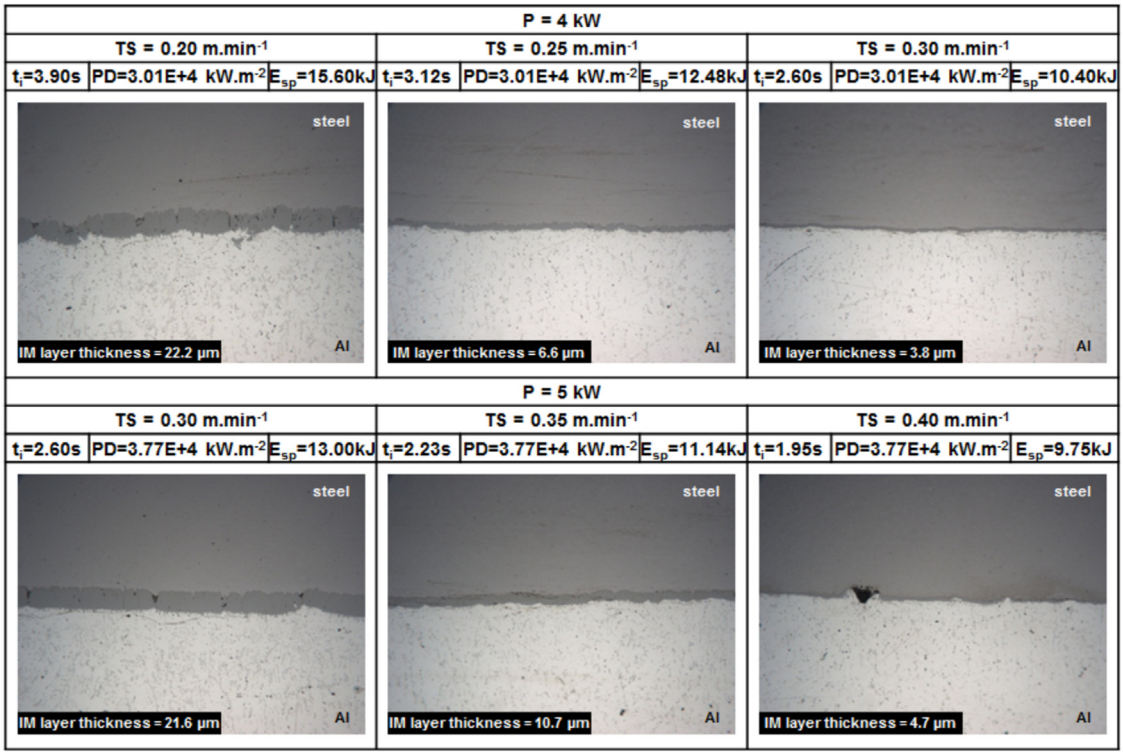

Fig. 9. Microscopic cross sectional view showing the IMC layer formed under different welding conditions and constant laser beam diameter of 13 mm

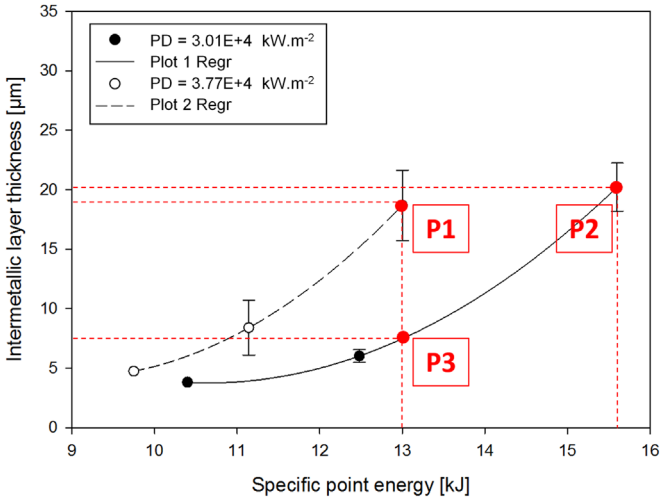

Fig. 10. Graph with results from steel to aluminium joints performed with laser welding process – IMC layer thickness vs Esp

Taking into account that E_{sp} is a function of *PD*, t_i and A_{beam} and considering in this case constant *PD* and A_{beam}, for each curve of uniform *PD*, the IMC layer thickness is actually a function of t_i (or *TS*, since A_{beam} is also constant). Therefore, higher E_{sp} values were obtained with higher t_i (heating time), result from welding with lower travel speed, which explains the thicker IMC layer for higher values of E_{sp}.

Fig. 10 highlights two points, P1 and P2, with similar IMC layer thickness formed under different energy levels $E_{sp,P1}$ and $E_{sp,P2}$, with $E_{sp,P1} < E_{sp,P2}$ (Fig. 10, eq. 4).

$$E_{sp,P1} = PD_{P1} \times t_{i,P1} \times A_{beam,P1} < PD_{P2} \times t_{i,P2} \times A_{beam,P2} = E_{sp,P2} \quad (4)$$

Considering the *FMIP*, the point P1 has higher PD and significantly lower t_i when compared to point P2, for the same A_{beam} (Eq. (5)). In terms of system parameters the point P1 was obtained with higher *P* and *TS*. This means that even with a lower t_i (or higher *TS*), the temperature generated by the higher *PD* is enough to produce the same IMC layer thickness. Therefore, using lower *PD* values it is possible to work in a larger range of t_i and keep the IMC layer thickness low.

$$\begin{cases} E_{sp,P1} < E_{sp,P2} \\ A_{beam,P1} = A_{beam,P2} = A_{beam} \\ PD_{P1} > PD_{P2} \\ t_{i,P1} \ll t_{i,P2} \end{cases} \quad (5)$$

The other important point is the acceleration of the IMC layer formation with increased *PD* values. Considering P1 and P3 (highlighted points in Fig. 10as an example, such that $E_{sp,P1} = E_{sp,P3}$ which can be written as shown in eq. 6.

$$E_{sp,P1} = PD_{P1} \times t_{i,P1} \times A_{beam,P1} = PD_{P3} \times t_{i,P3} \times A_{beam,P3} = E_{sp,P3} \quad (6)$$

From this equation and taking into account the individual FMIP, the following relation can be derived (Eq. (7)):

$$\begin{cases} E_{sp,P1} = E_{sp,P3} \\ A_{beam,P1} = A_{beam,P3} = A_{beam} \\ PD_{P1} > PD_{P3} \\ t_{i,P1} < t_{i,P3} \end{cases} \quad (7)$$

This equation shows again that for the same energy level and similar D_{beam}, the effect of using higher *PD* values is more important than the reduction on t_i on the growth of the IMC layer. This is even more evident when higher energy values are used. Thus, the

temperature seems to play a more important role than the time on the Fe-Al reaction. Therefore, it can be said with reasonable certainty that a thermal cycle with higher peak temperature would produce thicker IMC layer when compared to a longer thermal cycle but with lower peak temperature.

The IMC layer thickness, as observed from the experiments, ranges from 4 μm to 21 μm. According to [18] IMC layer thickness of up to 10 μm has been considered not harmful to obtain a sound joint.

The results of the mechanical tests are represented in Fig. 11 along with the evolution of the IMC layer thickness which has been previously analysed.

In both power densities (3.01E+4 and 3.77E+4 k W.m^{-2}) the mechanical shear tests showed similar strengths (although having a slight increase with E_{sp}) in all the experiments performed, even with the increase of IMC layer thickness. It can be explained by the fact that increasing the E_{sp} results in an increase in wetting area because of the longer thermal cycle (Fig. 12 shows the increasing of wetting area on steel side when the t_i and E_{sp} are increased). In the experimental region, initially the strength response is positive with increase in E_{sp} as higher wetted area has better impact on the joint strength than the adverse impact due to thicker IMC layer. The mechanical strength quickly reached a plateau and a decrease in strength is likely as further IMC layer growth would outweigh the advantage of higher wetting area. The failure was always observed at the Fe-Al interface and the maximum shear load bearing of approximately 30 kN (Fig. 11).

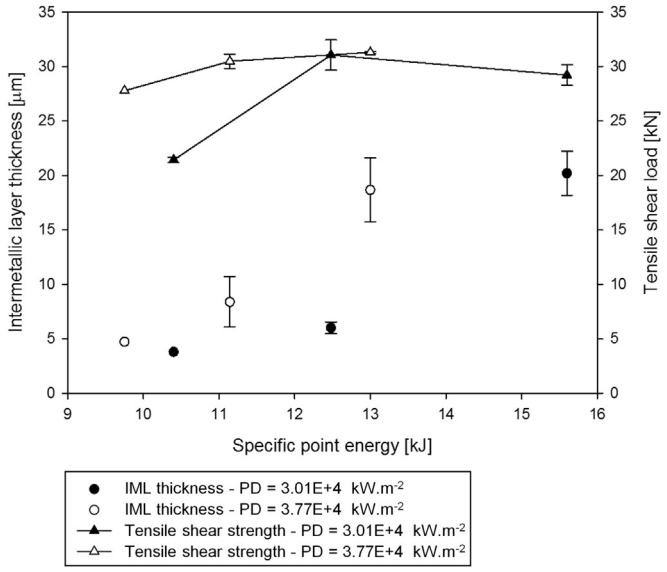

Fig. 11. Correlation between specific point energy, mechanical strength and IMC layer thickness

5. Conclusions

Laser welding-brazing has the capability of limiting the microstructural damage due to IMC formation as it allows aluminium to melt and wet the steel surface. Here it is worth noting that Al has some limited solid solubility in Fe, while Fe does not have any solubility in Al. Also diffusion is restricted when steel is in solid state and wetted by aluminium as compared to when both the alloys are in liquid state. The main conclusions are as follows:

- The study of the influence of the fundamental material interaction parameters on the IMC layer growth revealed exponential growth of IMC layer with E_{sp}. Powder density (PD) plays a vital role in determination of the IMC layer thickness and application of similar laser spot energy may result in thicker IMC formation for higher power density.
- In the current experimental situation, IMC layer thicknesses were observed to vary between 4–22 μm. The thickness data showed high quality welds in possible to manufacture using this route as IMC layer thickness below 10 μm is often referred to as an acceptable standard.
- The microstructure analysis showed the composite IMC layer composed of a needle shaped $FeAl_3$ on the Al side and a tongue shaped Fe_2Al_5 on steel side. The Fe_2Al_5 is much thicker as compared to $FeAl_3$.
- The tensile shear load on breakage observed to vary between 21.4 to 31.3 kN. All the samples exhibited interfacial failure in tensile shear testing.
- An initial increase in mechanical strength with specific point energy has been observed which can be attributed to the increase in wetting area with the increase in specific point energy. Although an increase in IMC layer thickness has also been observed in this range it seems the advantage owing to increase in wetting area outweighs the adverse impact from the increase in IMC layer thickness.

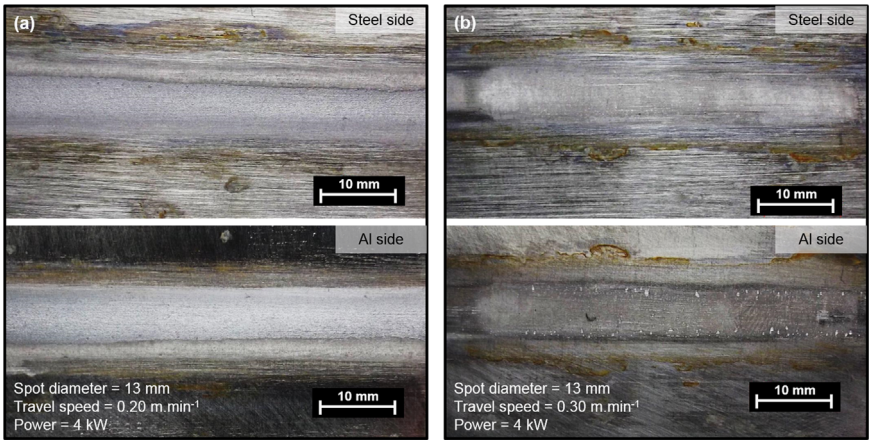

Fig. 12. Pictures of the Al-Fe interface after interfacial failure on the mechanical shear test. (a) PD=3.01E+4 k W.m-2; ti=3.9 s; Esp=15.6 kJ; (b) PD=3.01E+4 k W.m-2; ti=2.6 s; Esp=10.4 kJ

Acknowledgement

Dr. Supriyo Ganguly acknowledges the support by EPSRC through grant number EP/J017086/1. Sonia Meco is grateful to BAE Systems Naval Ships for providing financial support to this project.

References

[1] Bouche K, Barbier F. Coulet a. Intermetallic compound layer growth between solid iron and molten aluminium. Mater Sci Eng A 1998;249:167–75.
[2] Shahverdi HR, Ghomashchi MR, Shabestari S, Hejazi J. Microstructural analysis of interfacial reaction between molten aluminium and solid iron. J Mater Process Technol 2002;124:345–52.
[3] Fan J, Thomy C, Vollertsen F. Effect of thermal cycle on the formation of intermetallic compounds in laser welding of aluminum-steel overlap joints. Phys Procedia 2011;12:134–41.
[4] Akdeniz MV. the effect of substitutional impurities on the evolution of fe-Al diffusion layer. Science 1998;80-:46.
[5] Shih T, Tu S. Interaction of steel with pure Al, Al–7Si and A356 alloys. Mater Sci Eng A 2007;454-455:349–56.
[6] Lee W, Schmuecker M, Mercardo U, Biallas G, Jung S. Interfacial reaction in steel–aluminum joints made by friction stir welding. Scr Mater 2006;55:355–8.
[7] Taban E, Gould JE, Lippold JC. Dissimilar friction welding of 6061-T6 aluminum and AISI 1018 steel: Properties and microstructural characterization. Mater Des 2010;31:2305–11.
[8] Pl P. Explosion-bonded transition joints for structural pplications. Building 1989;3:64–72.
[9] Findik F. Recent developments in explosive welding. Mater Des 2011;32:1081–93.
[10] Acarer M, Demir B. An investigation of mechanical and metallurgical properties of explosive welded aluminum–dual phase steel. Mater Lett 2008;62:4158–60.
[11] Dharmendra C, Rao KP, Wilden J, Reich S. Study on laser welding–brazing of zinc coated steel to aluminum alloy with a zinc based filler. Mater Sci Eng A 2011;528:1497–503.
[12] Sierra G, Peyre P, Beaume FD, Stuart D, Fras G. Steel to aluminium braze welding by laser process with Al–12Si filler wire. Sci Technol Weld Join 2008;13:430–7.
[13] Mathieu A, Shabadi R, Deschamps A, Suery M, Matteı S, Grevey D, et al. Dissimilar material joining using laser (aluminum to steel using zinc-based filler wire). Opt Laser Technol 2007;39:652–61.
[14] Korte M, Stirn B, Laukant H, Wallmann C, Mu M, Haldenwanger H, et al. Fluxless laser beam joining of aluminium with zinc coated steel. Sci Technol 2005;10:219–26.
[15] Kreimeyer M, Wagner F, Sepold G. Development of a combined joining-forming process for aluminum-steel joints aluminum aluminum. ICALEO 2004;2004.
[16] Rathod M, Kutsuna M. Joining of aluminum alloy 5052 and low-carbon steel by laser roll welding. Weld J 2004:16–26.
[17] Ozaki H, Kutsuna M. Laser-roll welding of a dissimilar metal joint of low carbon steel to aluminium alloy using 2 kW fibre laser. Weld Int 2009;23:345–52.
[18] Schubert E., Zerner D.I., Sepold P.G. Laser beam joining of material combinations for automotive applications. SPIE 3097, lasers mater. process., vol. 3097, Munich: 1997, p. 212–21.
[19] Qiu R, Iwamoto C, Satonaka S. The influence of reaction layer on the strength of aluminum/steel joint welded by resistance spot welding. Mater Charact 2009;60:156–9.
[20] Qiu R, Iwamoto C, Satonaka S. Interfacial microstructure and strength of steel/aluminum alloy joints welded by resistance spot welding with cover plate. J Mater Process Technol 2009;209:4186–93.
[21] Qiu R, Satonaka S, Iwamoto C. Effect of interfacial reaction layer continuity on the tensile strength of resistance spot welded joints between aluminum alloy and steels. Mater Des 2009;30:3686–9.
[22] Qiu R, Shi H, Zhang K, Tu Y, Iwamoto C, Satonaka S. Interfacial characterization of joint between mild steel and aluminum alloy welded by resistance spot welding. Mater Charact 2010;61:684–8.
[23] Sierra G, Peyre P, Deschauxbeaume F, Stuart D, Fras G. Steel to aluminium key-hole laser welding. Mater Sci Eng A 2007;447:197–208.
[24] Yan S, Hong Z, Watanabe T, Jingguo T. CW/PW dual-beam YAG laser welding of steel/aluminum alloy sheets. Opt Lasers Eng 2010;48:732–6.
[25] Torkamany MJ, Tahamtan S, Sabbaghzadeh J. Dissimilar welding of carbon steel to 5754 aluminum alloy by Nd:YAG pulsed laser. Mater Des 2010;31:458–65.
[26] Borrisutthekul R, Yachi T, Miyashita Y, Mutoh Y. Suppression of intermetallic reaction layer formation by controlling heat flow in dissimilar joining of steel and aluminum alloy. Mater Sci Eng A 2007;467:108–13.
[27] Thomy C, Wagner F, Vollertsen F, Metschkow B. Lasers in the shipyard - Industrial laser solutions lasers in the shipyard - industrial laser solutions. Ind Laser Solut 2007:9–13.
[28] Suder WJ, Williams SW. Investigation of the effects of basic laser material interaction parameters in laser welding. J Laser Appl 2012;24:032009.
[29] Ion J. Laser processing of engineering materials: principles, procedure and industrial application. 1st ed. Oxford: Elsevier Butterworth-Heinemann; 2005.
[30] Hashemzadeh M, Suder W, Williams S, Powell J, Kaplan AFH, Voisey KT. The application of specific point energy analysis to laser cutting with 1 μm laser radiation, 8th International Conference on Photonic Technologies LANE 2014:1–9.
[31] Assuncao E, Williams S, Yapp D. Interaction time and beam diameter effects on the conduction mode limit. Opt Lasers Eng 2012;50:823–8.
[32] Nakamura S, Sakurai M, Kamimuki K. Detection technique for transition between deep penetration mode and shallow penetration mode in CO_2. J Phys D Appl Phys 2000;33:2941–8.
[33] Sánchez-Amaya JM, Delgado T, De Damborenea JJ, Lopez V, Botana FJ. Laser welding of AA 5083 samples by high power diode laser. Sci Technol Weld Join 2009;14:78–86.
[34] Sánchez-Amaya JM, Delgado T, González-Rovira L, Botana FJ. Laser welding of aluminium alloys 5083 and 6082 under conduction regime. Appl Surf Sci 2009;255:9512–21.
[35] Olsen FO. Hybrid laser Arc welding. hybrid laser-Arc Weld. 1st ed.CRC Press; 2009; 270–95.
[36] Kobayashi S, Yakou T. Control of intermetallic compound layers at interface between steel and aluminum by diffusion-treatment. Mater Sci 2002;338:44–53.

2015-04-01

Application of laser in seam welding of dissimilar steel to aluminium joints for thick structural components

Martins Meco, Sonia Andreia

Elsevier

Meco S, Pardal G, Ganguly S, et al., (2015) Application of laser in seam welding of dissimilar steel to aluminium joints for thick structural components, Optics and Lasers in Engineering, Volume 67, April 2015, pp. 22-30

http://dx.doi.org/10.1016/j.optlaseng.2014.10.006